Predicting Cloud-to-Ground and Intracloud Lightning in Weather Forecast Models

BARRY H. LYNN

Weather It Is Ltd., Efrat, Israel

YOAV YAIR

Department of Life and Natural Sciences, Open University of Israel, Ra'anana, Israel

COLIN PRICE

Department of Geophysical, Atmospheric, and Planetary Sciences Tel Aviv University, Tel Aviv, Israel

GUY KELMAN

Weather It Is Ltd., Efrat, Israel

ADAM J. CLARK

NOAA/National Severe Storms Laboratory, Norman, Oklahoma

(Manuscript received 22 November 2011, in final form 13 June 2012)

ABSTRACT

A new prognostic, spatially and temporally dependent variable is introduced to the Weather Research and Forecasting Model (WRF). This variable is called the potential electrical energy (E_p). It was used to predict the dynamic contribution of the grid-scale-resolved microphysical and vertical velocity fields to the production of cloud-to-ground and intracloud lightning in convection-allowing forecasts. The source of E_p is assumed to be the noninductive charge separation process involving collisions of graupel and ice particles in the presence of supercooled liquid water. The E_p dissipates when it exceeds preassigned threshold values and lightning is generated. An analysis of four case studies is presented and analyzed. On the 4-km simulation grid, a single cloud-to-ground lightning event was forecast with about equal values of probability of detection (POD) and false alarm ratio (FAR). However, when lighting was integrated onto 12-km and then 36-km grid overlays, there was a large improvement in the forecast skill, and as many as 10 cloud-to-ground lighting events were well forecast on the 36-km grid. The impact of initial conditions on forecast accuracy is briefly discussed, including an evaluation of the scheme in wintertime, when lightning activity is weaker. The dynamic algorithm forecasts are also contrasted with statistical lightning forecasts and differences are noted. The scheme is being used operationally with the Rapid Refresh (13 km) data; the skill scores in these operational runs were very good in clearly defined convective situations.

1. Introduction

Over the past 50 years, almost 5000 people have died in the United States from lightning strikes (Ashley and Gilson 2009). Moreover, lightning kills on average more people in the United States than tornadoes and hurricanes, but fewer than flash floods (Curran et al. 2000; Holle et al. 2005; Ashley and Gilson 2009). Lightning has been and is clearly a hazard (e.g., American Meteorological Society 1924a,b; Lopez and Holle 1995; López et al. 1995; Rorig and Ferguson 2002; Holle et al. 1996; Hodanish et al. 2004; Holle et al. 2005; Wallmann et al. 2010; Schultz et al. 2009). Hence, the need for effective,

Corresponding author address: Prof. Yoav Yair, Dept. of Life and Natural Sciences, Open University of Israel, 1 University Rd., Ra'anana 43107, Israel.
E-mail: yoavya@openu.ac.il

DOI: 10.1175/WAF-D-11-00144.1

reliable lightning prediction is therefore a clear requirement, especially for vulnerable sectors such as agriculture, energy, recreation, and aviation.

Lightning types are generally referred to as either cloud to ground (CG, with positive or negative polarity) or intracloud (IC) (MacGorman and Nielson 1991; Branick and Doswell 1992; Shafer et al. 2000; Kuhlman et al. 2006). Lang et al. (2004) provide a summary of percent peak positive flash rates for different storm types [as a percentage of positive (+CG) and negative (−CG) cloud-to-ground lightning].

Current lightning observation networks are technically advanced (see review in section 6.10 of MacGorman and Rust 1998; Price 2008) and are used to make nowcasts of lightning strikes (e.g., Stern et al. 1994; Short et al. 2004; Saxen et al. 2008; Kohn et al. 2010). In contrast, Yang and King (2010) used radar reflectivity as a predictor of short-term lightning [see also Hondl and Eilts (1994), Gremillion and Orville (1999), Mosier et al. (2011), and Seroka et al. (2012)]. However, until recently, non-near-term operational forecasts of lightning relied on thermodynamic instability parameters [such as the lifted index, K index, convective available potential energy, and the cloud physics thunder parameter; Bright et al. (2005)]; that is, there was very little reference to cloud microphysics and/or charge separation processes [see also Price and Rind (1994), Mazany et al. (2002), Burrows et al. (2005), Shafer and Fuelberg (2008), and Wallmann et al. (2010)].

Recent advancements in lightning prediction have occurred. The National Severe Storm Laboratory (NSSL) produces near-real-time hourly total lighting threat forecasts with 36-h lead times. Their lightning predictions are based on the work of McCaul et al. (2009), who used the model-derived graupel flux in convective clouds with the total ice content to obtain a statistical relationship between these two parameters and the total lightning flash density. Dahl et al. (2011) developed another scheme based on identifying convective cells in forecasts and then initiating lightning when the ''critical electric field strength'' reaches a certain threshold value. Yair et al. (2010) describe the development and utilization of the lightning potential index (LPI; J kg^{-1}), a new index for evaluating the potential for charge generation leading to lightning activity derived from weather forecast model output. Building on this work, Lynn and Yair (2010) provided a statistical approach to predicting lightning density of cloud-to-ground and total lightning.

The lighting prediction schemes in McCaul et al. (2009) and Lynn and Yair (2010), like other statistical approaches, assume that the number of lightning flashes depends on some temporal and spatial averages of parameters derived from the model fields. Such an assumption introduces potential errors in predicting the number of lightning flashes because convective clouds develop over different time scales and move at different speeds from location to location, depending on the background environmental conditions.

For these reasons, we were motivated to adopt a dynamic approach to predicting lightning in convection-allowing[1] models. We chose to parameterize charging processes within clouds, and use this parameterization to calculate a temporally and spatially dependent variable [the electrical potential energy, E_p (J)] associated with the charging processes operating within thunderclouds. The value of E_p grows in magnitude as the clouds build up and separate electrical charge, and it is advected within the weather forecast model grid like any other four-dimensional variable. When it exceeds threshold values, E_p is converted into electrical energy, immediately dissipating the energy as lightning strokes (cloud-to-ground and intracloud lightning) and reducing the magnitude of E_p at that grid point accordingly. Note, our approach does not explicitly calculate lightning because the actual electric field is not directly computed from the microphysics (e.g., as in Helsdon and Farley 1987; Scavuzzo and Caranti 1996; MacGorman et al. 2001; Mansell et al. 2002; Kuhlman et al. 2006; Barthe and Pinty 2007; Pinty and Barthe 2008; Mansell et al. 2010; Fierro et al. 2007, 2008).

2. Description of the lightning prediction scheme

The development of the lightning parameterization scheme begins with the utilization of the LPI (Yair et al. 2010). The LPI is a measure of the capability for charging within clouds. In Yair et al. (2010), the LPI is calculated within the charge separation region of convective clouds between 0° and −20°C, where the noninductive mechanism by collisions of ice and graupel particles in the presence of supercooled water is most effective (Saunders 2008, Mansell et al. 2010). The LPI has its largest values in the presence of strong vertical velocities (see van den Broeke et al. (2005)), when graupel exists in equal ratios relative to snow, ice, and water. When it is equal to one, it indicates that the relative ratios of water, ice, snow, and graupel are such that the potential for charging is maximized in strong updrafts [in accordance with the description of Saunders (2008)].

[1] Convection allowing generally refers to simulations run using grid spacing at or below 4 km, which is about the coarsest grid spacing at which dominant circulations within midlatitude mesoscale convective systems can be adequately depicted (Weisman et al. 1997).

The LPI is equal to αw^2, where the variable w is the vertical velocity,

$$\alpha = 2(q_{\text{if}}q_l)^{0.5}/(q_{\text{if}} + q_l), \tag{1}$$

q_l is the total liquid water-mass-mixing ratio, and q_{if} is the ice fractional mixing ratio in kilograms per kilogram defined by

$$q_{\text{if}} = q_g\{[(q_s q_g)^{0.5}/(q_s + q_g)] + [(q_i q_g)^{0.5}/(q_i + q_g)]\}. \tag{2}$$

The variables q_g, q_i, and q_s are the graupel, ice, and snow mixing ratios (kg kg^{-1}), respectively. Note that in Yair et al. (2010) α was referred to as ε, but ε is often used as the variable for the permittivity of the atmosphere so this is now changed from its previous designation.

It is proposed that the LPI (αw^2) times the mass of ice divided by a unit coulomb of charge C represents the electrical potential of the cloud fields. The units of this electrical potential are volts (V, J C^{-1} kg$_{\text{air}}^{-1}$):

$$V = C^{-1}(q_g + q_i + q_s)\alpha w^2. \tag{3}$$

As charging continues in clouds, it will build up potential electric energy (E_p).

The source term for the potential electric energy is referred to here as the power index (P, W m^{-3}). It is proposed to be the same as that for the ''classical'' electrical power equation, multiplied by ρ (the density of air, kg m^{-3}):

$$P = \rho IV, \tag{4}$$

where the current I (A) is given by

$$I = Q/t. \tag{5}$$

Here, Q is the electric charge in coulombs and its value is chosen such that the appropriate amount of energy will build up over several model time steps and then be discharged during the time interval (t) of a lightning event propagating from the height of discharge to the ground as a vertical leader. [see Krehbiel et al. (2008), who also chose a charging parameter to calculate the buildup of electric charge]. The time scale depends on the layer in which the energy begins to be discharged. It is largest for +CG and smallest for IC. A lightning event can be either a positive or negative CG stroke or an IC lightning discharge that occurs in t milliseconds.

In terms of the actual calculations on the atmospheric model grid, the grid-scale source of potential electrical energy is

$$E_S = P\Delta t\Delta x\Delta y\Delta z, \tag{6}$$

where Δt is one lightning algorithm time step, and the variables Δx, Δy, and Δz are the grid dimensions in the x, y, and z (vertical) directions, respectively [the vertical dimension corresponds to the full sigma levels in the Weather Research and Forecasting Model (WRF)]. The dissipation of electrical energy (E_D) associated with N number of lightning stroke events is

$$E_D = -NT, \tag{7}$$

where T is a threshold energy and is the average threshold energy present in one lightning stroke. When $E_p > T$, the number of lightning events N is calculated from the potential energy as

$$N \approx E_p/T. \tag{8}$$

The equation is ''approximate'' because not all energy is necessarily dissipated for each lightning event because N is an integer value.

The threshold energy depends on the type of lightning event that occurs (+CG/−CG or IC). For instance, the energy threshold for positive lightning is assumed to be half an order of magnitude larger than for negative cloud-to-ground or cloud lightning. Note, when we speak about threshold values, we are not referring to the threshold for electrical breakdown, where the value for +CG should be lower than −CG because this threshold is inversely proportional to pressure. Rather, the threshold is based on the assumption that the value of the average peak current for +CG is larger than −CG and reflects the total energy stored in the electric field. As we note below, the +CG events are assumed to occur from the anvil or upper part of the cloud, and hence the discharge of energy is larger than occurs with −CG events. Hence, we are not explicitly forecasting +CG events that might occur from that part of the cloud closer to the surface.

When an event happens and a threshold for either lightning type is surpassed, the total amount of energy that is dissipated, E_D (J), for that lightning event is specifically calculated for each model atmospheric column is

$$E_D = -\sum\min(E_p, E_{Dg}), \tag{9}$$

where E_{Dg} (J) is the amount of energy within each grid volume element. Although specific charging layers are specified, we integrate and discharge from the top of the atmospheric column and proceed with the integration toward cloud base, removing only enough

energy equivalent to the energy of the number of lightning events that occurred. We integrate over the whole column because energy can be advected or diffused outside the charging layers. Any (positive) residual energy is distributed equally between the grid levels in the charging zone.

Through the formulation of a four-dimensional (x, y, z, t) derivative equation, we implicitly account for energy buildup in convective and stratiform clouds as well as its possible advection from convective to stratiform clouds (Rutledge et al. 1990; Schuur et al. 1991; Nielsen et al. 1994; Parker et al. 2001). We refer to this formulation as the dynamic approach to predicting lightning. The equation for the Lagrangian (total derivative) comoving frame of reference is

$$dE_p/dt = E_S + E_{Dg} + E_T. \tag{10}$$

Here, d/dt can be transformed from the Lagrangian comoving frame of reference to the grid-cell Eulerian form,

$$\partial E_P/\partial t + \mathbf{U} \cdot \nabla E_P = E_S + E_{Dg} + E_T, \tag{11}$$

and E_T is the diffusion due to turbulent processes. Because the variable E_p is a total derivative, any remaining energy after lightning occurs can be redistributed to produce additional lightning activity. Note that the variable E_p was transformed to an energy density (by dividing by density) before being passed out of the lightning algorithm to the advection scheme, and then transformed back after the advection through multiplying by density before calculating new values of E_p.

Equations (1)–(10) were coded into an algorithm that prognosticates the potential energy associated with each lightning type: positive cloud to ground (E_{p+}), negative cloud to ground (E_{p-}), and intracloud (E_{pic}). Each set of coded equations has its own set of variables, and there are actually three four-dimensional variables added to the registry: $E_{p+\text{cg}}$, $E_{p-\text{cg}}$, and E_{pic}. There are also power indices (P_+, P_-, and P_{ic}) with corresponding charging coefficients (Q_+, Q_-, and Q_{ic}) and threshold values (T_+, T_-, and T_{ic}). Values of parameters used in the model simulations are provided in Table 1. To reduce computational expense, the time step Δt, was chosen to be 6 times the length of the standard model forecast time step, which was 20 s. Hence, the lightning algorithm was called every 120 s, but energy was advected according to the model forecast time step of 20 s. However, a test comparing forecast results calling the lightning routine every time step showed only small changes in the results (but added a couple of minutes of computer time over a 14:25-min simulation on one of our computers used for research simulations).

TABLE 1. Values of parameters used in the model simulations. The Q is the number of coulombs transferred during 1 s, while t is the time it takes for a stroke to occur. It is assumed that lightning bolts travel at 60 000 m s^{-1}. The value of t is approximate because the actual time for the lightning event depends on the height of the −27° and −2°C isotherms, as described in the text. Note that T is the threshold energy for a stroke or lightning event to occur, and T_{z+} and T_{z-} indicate the bounds of the charging levels.

Variable	+CG	−CG	IC
Q (C)	0.5×10^{-4}	0.5×10^{-4}	0.5×10^{-4}
t (s)	0.12	0.06	0.03
T (J)	5×10^{9}	1×10^{9}	1×10^{9}
T_{z-} (°C)	−10	0	0
T_{z+} (°C)	−30	−20	−30

Throughout these calculations, we assume a typical orientation for charging separation in clouds: a double dipole (e.g., Kuhlman et al. 2006, their Fig. 1) with positive charges predominant in the upper half of the cloud and negative charges predominant in the bottom half of the cloud. The assumption is that negative, positive, and intracloud flashes neutralize different energy ''sources'' within overlapping layers defined by the temperature at the top of each layer T_{z+} and bottom T_{z-}. For instance, negative cloud-to-ground flashes neutralize negative charges in the lower part of the cloud and positive charges at the ground. The origin for −CG is assumed to be the first model layer in a cloud below the height of the −2°C isotherm. The time scale for −CG is determined from the model height immediately below −2°C divided by the assumed speed of lightning leaders [~60 km s^{-1}; Rakov and Uman (2003)]. Positive cloud-to-ground lightning neutralizes positive charges located in the upper part of the cloud and negative charges on the ground. The origin of +CG is the first model layer below −27°C. Intracloud lightning neutralizes positive and negative charges within clouds, and the time scale of IC events is ½ the difference between the time scale for +CG and −CG.

The implication of this simplified separation of charges is that stronger convective cells (with deeper mixed-phase regions) should have more positive flashes than weaker convective cells. This assumption is consistent with the findings of Stolzenburg (1994), who showed that a high rate and a high percentage of positive cloud-to-ground flashes were associated with exceptionally tall and rapidly growing storms (see also Fierro et al. 2006). Likewise, weaker and less rapidly growing storms tend to produce a much higher percentages of negative cloud-to-ground flashes (MacGorman and Nielson 1991).

Yet, the reader should keep in mind that cloud systems may have at different times monopole, diplole, and tripole charge structures (e.g., Williams 1989; Kitagawa and Michimoto 1994), and clouds with inverted dipoles may not produce any cloud-to-ground lightning at all [even though they can still produce many intracloud lightning flashes; Tessendorf et al. (2007)]. Dipole structures without CG flashes were also noted by Qie et al. (2005) and Wiens et al. (2005). Hence, the present parameterization cannot be inclusive of all electrical configurations in thunderstorms.

3. Experimental setup

a. The Weather Research and Forecasting Model (WRF)

The WRF is used by many operational services for short- and medium-range weather forecasting. It is a fully compressible, nonhydrostatic atmospheric model, using a terrain-following hydrostatic vertical pressure coordinate. In recent years it has also become an accessible research tool, as it offers multiple physics options that can be flexibly combined in many ways [full formulation and documentation can be accessed through the University Corporation for Atmospheric Research (UCAR) website http://www.mmm.ucar.edu/wrf/users/pub-doc.html].

For the case studies and sensitivity tests, we used version 3.2 of the WRF. For a series of operational forecasts, we used version 3.3. Based on positive results presented in Givati et al. (2012), we used the WRF single-moment six-class microphysical parameterization (WSM6), a single moment scheme with cloud water and rainwater, ice, snow, and graupel (Dudhia et al. 2008). This scheme predicts cloud mass, ice particle mass, and the hydrometeors of snow and graupel, but there is no explicit prediction of hail. The coarse grid also used the Kain–Fritsch convective scheme (Kain and Fritsch 1993; Kain 2004). The shortwave radiation scheme was that of Dudhia (1989), while the longwave radiation scheme was that of Mlawer et al. (1997). The Noah land surface model (LSM) outlined in Chen and Dudhia (2001a,b) was used to simulate surface fluxes. The boundary layer scheme used was that of Mellor–Yamada–Janjić (MYJ; Mellor and Yamada 1982; Janjić 2002).

Four case studies were initially simulated using Rapid Update Cycle (RUC2) forecast data with 13-km grid spacing. RUC2 data were used instead of Global Forecast System (GFS) data in order to improve the initialization of moist convection. The RUC [like the Rapid Refresh (RAP) model] assimilates radar reflectivity data. Radar reflectivity assimilation is probably the most important reason why the RUC (and now the RAP) do somewhat better than the GFS initially (Weygandt et al. 2008). A secondary reason probably is the higher horizontal resolution of the RUC data (13 km) versus the GFS (½°). The case study days and hours were (a) 1200 UTC 16 April–0600 UTC 17 April 2011, (b) 1200 UTC 19 April–1200 UTC 20 April 2011, (c) 1800 UTC 22 April–0600 UTC 23 April 2011, and (d) 1200 UTC 27 April–0600 UTC 28 April 2011. The RUC2 forecast data from 0000, 0600, 1200, or 1800 UTC starting times are available for 12 h of forecast simulation. When the simulation extended beyond 12 h, we used 12-hourly forecasts of subsequent RUC forecast runs to fill in the boundary conditions for the WRF forecasts.

Each of these case study days had severe weather. For example, case study a had 139 tornado reports, 215 wind reports, and 67 hail reports recorded by the Severe Storm Prediction Center (SPC). Many of the tornadoes were located near Charleston, South Carolina. Case study b had 77 tornado reports, 552 wind reports, and 357 hail reports. For the case beginning on 22 April, there were 29 tornadoes and 200 hail reports (again recorded by the SPC); many of the tornadoes were located near the city of St. Louis, Missouri. Case d had 259 tornado reports, 335 wind reports, and 300 hail reports. An additional 24-h case study from the winter of 2012, with a relatively small number of severe storm reports, was done for 4 February 2012.

Various sensitivity tests were done for the case study of 27 April to 1) investigate the possible impact of graupel versus hail on lightning forecasts (using GCE microphysics) and 2) the possible impact of improved data assimilation on the accuracy of forecast lightning. For investigation of the impacts on the forecasts, two experiments were done: the first with the microphysics set on its graupel settings, and the next on its hail settings. For the data assimilation impact, 13-km RAP data from 1200 UTC were used instead of RUC2 data, and then GFS data were used in a second simulation. The RAP has a newer hourly update system that replaces the RUC's hourly update system (S. Benjamin 2012, personal communication) and, hence, we would expect better initialization of the atmospheric state.

In these case study tests, there was only a single 448 × 448 with 4-km grid spacing domain in all of the forecasts. The center of the domain was moved within the eastern United States depending on the location of the severe weather. However, an additional forecast was done using 3-km grid spacing to test the possible sensitivity of the forecast algorithm to changes in grid spacing from 4 to 3 km. Here, 597 × 597 grid elements were used.

Additionally, skill statistics are presented from six operational forecasts produced from January 2012 until March 2012. These forecasts were made using WRF

version 3.3, and they occurred 4 times daily, every 6 h, and forecasts that cover the central and eastern United States are displayed online (www.lightning-forecast.com). These days were chosen because they have a range of lightning signatures corresponding to midlevel warm-air advection, frontally forced convection, and severe weather associated with organized cellular convection. These forecasts are initiated with hourly RAP reanalysis data for the 3 h preceding the forecast. The WRF four-dimensional data assimilation (FDDA) is used to nudge the model forecast. After the spinup, most of the forecasts proceeded for 18 h (depending on available computer resources) using 3-hourly RAP data, but without FDDA. In these case studies, the forecasts beginning at 0000 UTC were used and cover the hours 0300 to 2100 UTC of the same day.

b. *Lightning data*

Two sets of lightning data were used. The first is from the U.S. Precision Lightning Network (USPLN) and was provided courtesy of WSI Corporation. It is a full-stroke network. The strokes are defined as either positive cloud to ground, negative cloud to ground, or intracloud (or cloud lightning).

The USPLN measurements are made with TOA Systems Inc.'s Precision Lightning Sensor (PLS), which utilizes time-of-arrival technology. The PLS is a broadband receiver. This allows it to capture a substantial amount of the lightning energy, which enables it to distinguish between cloud-to-ground lightning and intracloud lightning. The PLS uses commercial GPS timing as a reference and has an accuracy of 15 ns. The timing is constantly monitored and corrected, resulting in more accurate lightning locations. PLS sensors utilize proprietary low-frequency detection methods and waveform discrimination to allow the network to calculate and display the location where the stroke hits the ground.

The raw lightning data from the PLS sensors are passed to the Advanced Stroke Processor (ASP), which is preprogrammed to contain information related to the particular sensor sites and system-specific mathematical and physical coefficients. The efficiency of the network for CG lightning is estimated at ~95%, but the efficiency of the IC observations is estimated to be only 15%. Hence, our analysis using this data will emphasize the observed CG lightning versus predicted CG lightning, rather than IC.

The second set of lightning data is from Earth Networks, a relatively new dataset for CG and IC lightning. It was used to obtain a better evaluation of the intracloud lightning forecast. The Earth Networks Total Lightning Network (ENTLN) uses adaptive digital filtering in an effort to reduce local noise, allowing the individual sensors to adapt to their local environment. The Earth Networks Lightning Sensors detect lightning over a wide frequency range of 1–12 MHz, employing two analog to digital converters. The lowest frequencies are utilized for long-range detection, the middle frequencies are used for locating CG strokes, while the highest frequencies are useful in locating a significant portion of fast cloud pulses. Earth Network notes that the detection of in-cloud lightning is critical in severe weather prediction and advance warning of large hail, gusty winds, heavy rainfall, and even tornadoes (see also Schultz et al. 2009). Earth Networks claims that the IC detection is greater than 60% over much of the eastern United States and as much as 80% in some areas. The CG detection rate is claimed to be >95% over the entire eastern United States, but less elsewhere; probably because of the denser detector deployment there.

4. Results

a. *General results*

The observed lightning pattern for each case study was compared to the forecast lightning pattern. Through this comparison, we visually noted that the structure, position, and relative magnitude of the forecast lightning corresponded fairly well with the observed lightning fields. From this, we deduced that the forecasts were suitable for comparison and evaluation of the lightning forecast algorithm.

Figure 1 shows the total number of observed and forecast lightning events for four case study days. The results show strong predictability of the total IC and total CG lightning. On each of the days, the predicted total IC values are larger than the observed IC values. This is desired, given that Earth Networks claim of measuring about 70%–80% of the actual IC. The forecast total CG each day was very similar to the observed CG, where the network observes about 95% of the actual CG lightning.

The data in Fig. 2 show that each case study had the largest number of observed −CG lightning events within the first range of values ($1 \leq \# < 3$), and an observed secondary maximum located in the range $5 \leq \# < 10$. Each forecast reproduced the magnitude of the number of lightning events in all ranges quite well, including the secondary maximum within the range $5 \leq \# < 10$. Positive CG strokes were recorded on each case study day, but in numbers much lower than for the −CG strokes (Fig. 3). Most of the gridded positive lightning events were observed to occur in the range $1 \leq \# < 3$, and the values shown were well predicted. On 19 and 22 April +CG lightning strokes within other ranges were also recorded, and these were also predicted with the dynamic algorithm. On all days, the observed and predicted

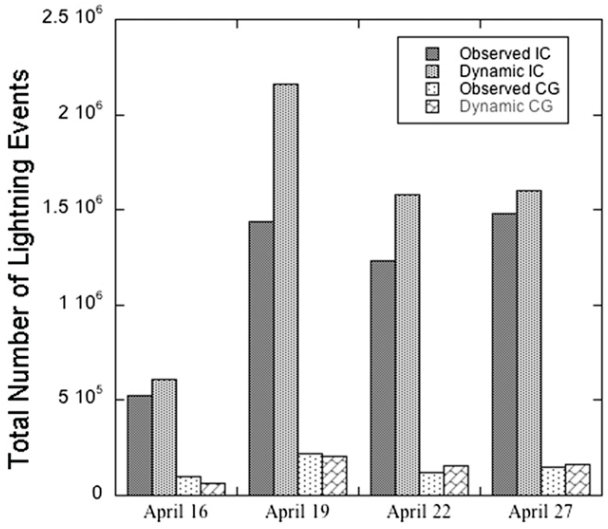

FIG. 1. Total number of lightning events for four case study days. The Earth Networks IC observations and USPLN's CG lightning network are plotted vs forecast values.

histograms of IC values show a good match, taking into account that between 70% and 80% of the IC lightning is actually observed.

For the case study beginning 1800 UTC 22 April, Figs. 2–4 also show the predicted number of −CG, +CG, and IC events from the dynamic algorithm, but without including the advection of potential energy (E_p) from one grid element to the next. Instead, energy was either converted to lightning (if it exceeded the threshold values) or it was lost; that is, E_p was set to zero when exiting the lightning algorithm. This approach is one that might be taken to use a parameter like the power index by itself or an approach similar to that of Dahl et al. (2011).

The values of the plotted histograms calculated without advection of E_p were smaller in magnitude compared to the forecast with the dynamic algorithm that included the advection of energy from one grid to another. This was especially so in the range $1 \leq \# < 3$ for each type of lightning. It is this range of lightning values that is most susceptible to changes in the advection of E_p. Of the three types of lightning, the biggest impact of assuming that all energy was generated and dissipated in a single time step was on the prediction of +CG, where most of the values of +CG in the histogram plot are concentrated. This is because energy must be generated and then transferred to the anvil regions of the convective storms to produce many of the +CG events.

b. More specific results

The day with the greatest number of tornadoes was the case study that started 1200 UTC 27 April 2011 (i.e., the Tuscaloosa, Alabama, tornado event) and finished at 0600 UTC 27 April. We analyze these day's results in detail, but we note that the conclusions apply generally to the other three case study days.

The convection that led to the severe weather began as a relatively weak area of total lightning entering northern Mississippi and Alabama. SPC recorded tens of hail and high wind events, but there were only five tornado reports (not shown). Between 1800 and 2100 UTC, total lightning values rose and the number of tornado reports (90) exceeded the number of wind and hail reports (for brevity, again not shown). The reported tornadoes were in two west-to-east lines stretching from northern Mississippi into northern Alabama. There were elevated lightning values in many locations where tornadoes were also reported. In fact, many of these tornadoes occurred in areas with greater than 50 total lightning events per 3-h period. The forecast lightning (as noted; not shown) was suggestive of the potential for severe weather in areas of enhanced forecast lightning values, but the forecast position was a bit farther northwest of the actual locations owing to the spinup time required for this forecast from a "cold start."

Observed total lightning rose dramatically between 2100 and 0000 UTC 28 April in the next 3 h as the severe weather moved to the east-northeast (Fig. 5). There were more tornado reports (82) than hail and strong wind reports, and Fig. 5 shows that many of these occurred in areas with between 125 and 250 lightning events per 3-h period and higher. The forecast total lightning (Fig. 5) corresponds both spatially and in magnitude with the observed lighting, and is strongly indicative of the potential for severe weather in many of the areas indicated by the observations.

From 0000 to 0300 UTC 28 April, the storms moved off to the northeast, and the number of tornado reports (64) was about equal to the hail and wind reports, while the maximum lightning values shown were about half what they were before (not shown). The forecast lightning for the same period very nicely matched the observed spatial distribution of lightning.

The total lightning was averaged in a circular area with 300-km radius around the city of Tuscaloosa. The time rate of change for the forecast lightning matches the time rate of change of the observed total lightning (Fig. 6), with the lightning entering this circular area and the peak occurring about 11 h into the forecast (about 2300 UTC 27 April).

Figure 7 shows vertical cross sections of E_{p+}, E_{p-}, and E_{pic}, as well as the vertical velocity. The vertical cross section extends west to east at latitude 32.32°, and is centered in western Alabama, while the convection within is moving west to east. The vertical velocity field

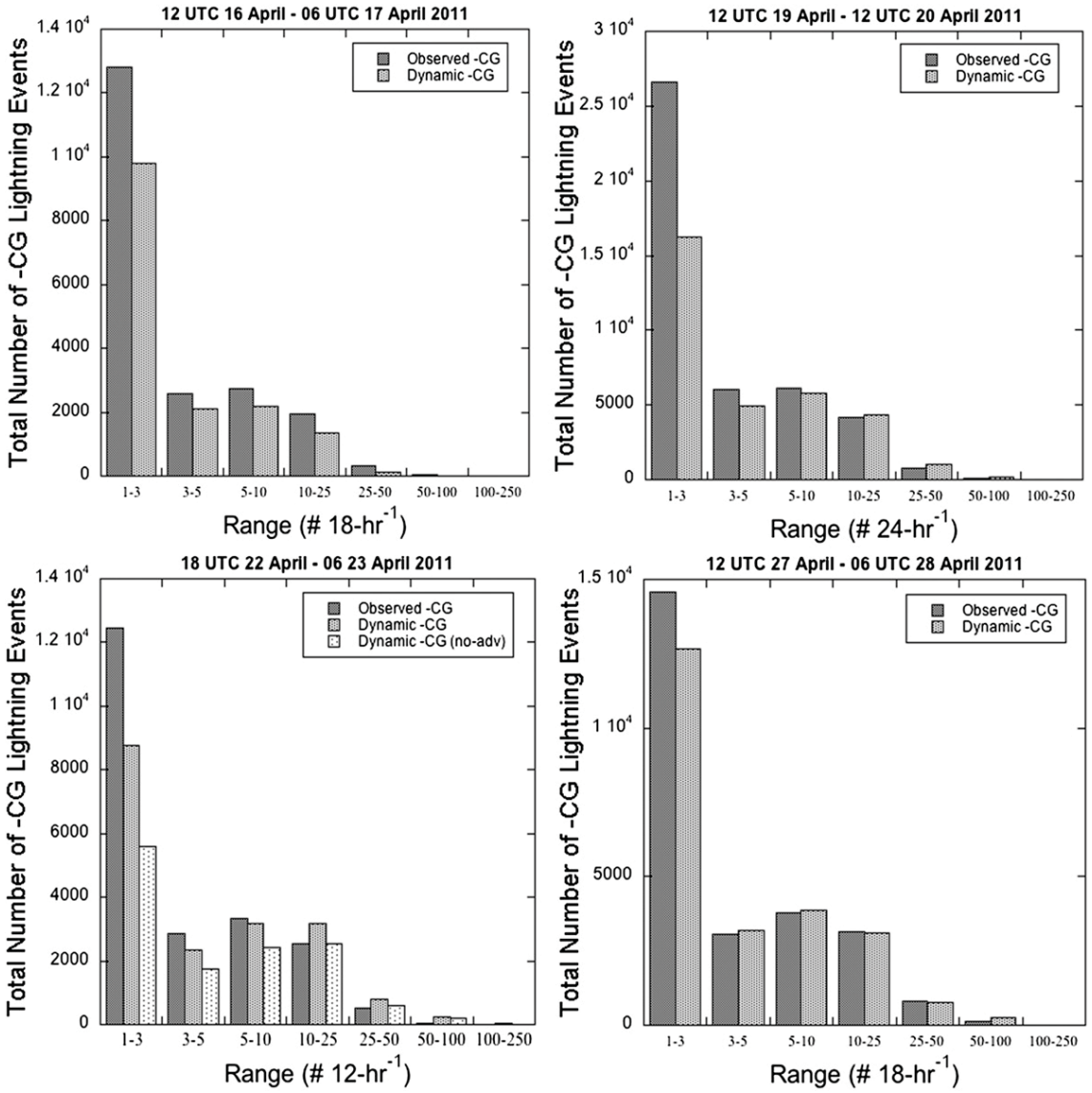

FIG. 2. Observed vs forecast −CG lightning events for four case study days. The number of −CG lightning events on each 4-km grid element were binned according to the ranges shown on the x axis.

shows a main convective core (with $w > 32$ m s^{-1}), trailed by a midtropospheric convective core of somewhat smaller, but still significant, and positive vertical velocities ($w > 10$ m s^{-1}). The former is located just east of −89° longitude, while the latter is just west of 89° longitude. There are also areas of positive vertical velocity to the rear of the convective cores (near 12 km in height), most likely associated with upper-level stratiform and/or anvil clouds. ($0.1 \leq w < 2$ m s^{-1}). Weak areas of positive vertical velocity, of large depth, most likely associated with stratiform–anvil cloud development ($w < 1$ m s^{-1}), extend quite a ways ahead of the main convective area.

The vertical cross section of E_{p+} has a maximum at about 10 km and clearly shows higher values of E_{p+} in the main convective (vertical velocity) core and in the shape of the anvil-like clouds east of the main core (which is actually above the assumed charging layer). There are also pockets of elevated values of E_{p+} in the secondary core and in the upper-level anvil cloud to the west of the main core. The parameters E_{p-} and E_{pic} are apparent as two columns, rather than as one in the E_{p+} cross section. The high vertical extent of these energy columns is due to advection of them within the main and secondary strong updrafts. The trailing column of E_{p-} and E_{pic} corresponds spatially to the midlevel

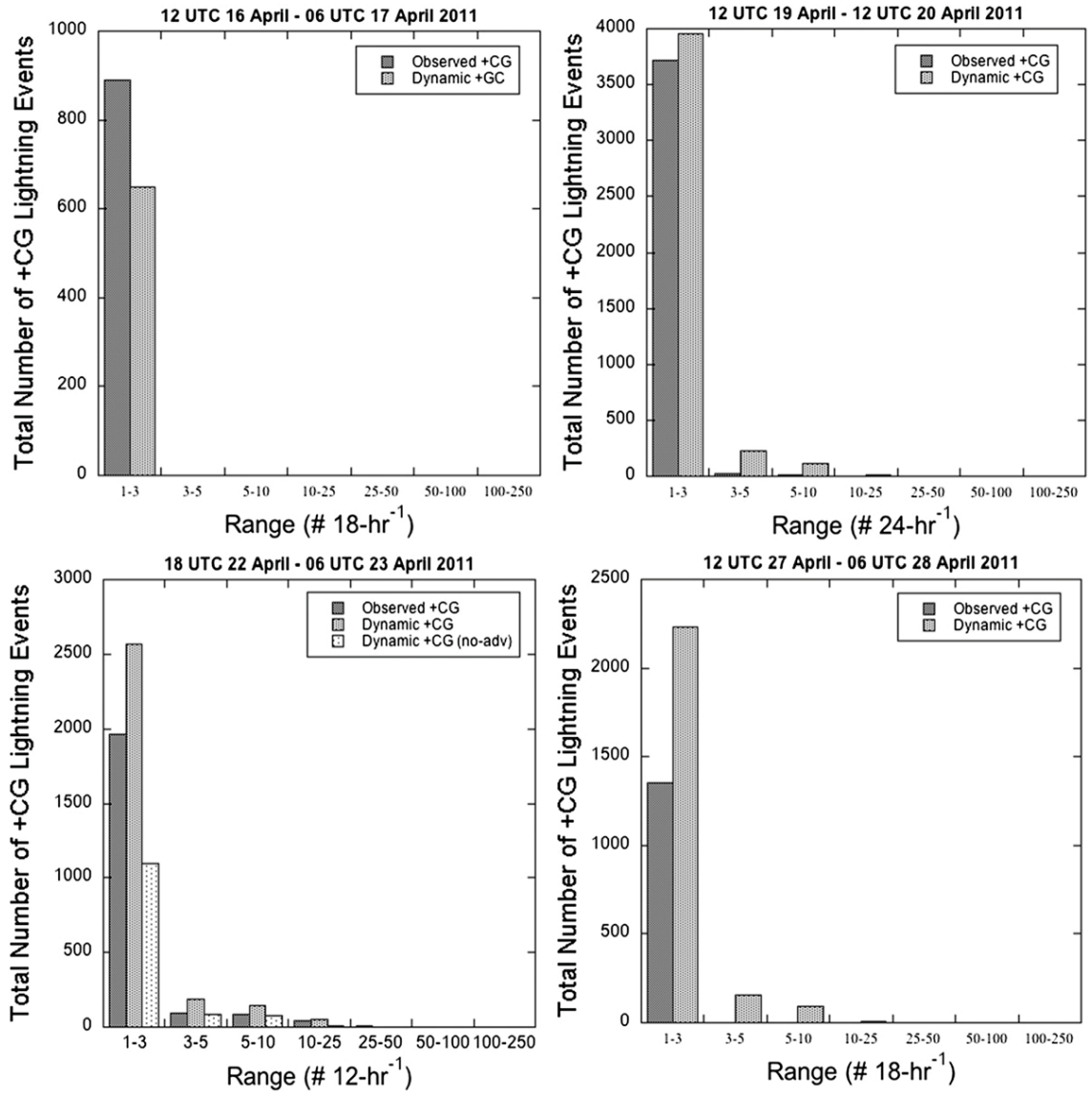

FIG. 3. As in Fig. 2, but for observed vs forecast +CG.

convective core (as indicated by the vertical field). Elevated values of E_{p-} and E_{pic} exist in the anvil/stratiform area west and east of the main convective core. Comparing these fields with that of E_{p+} strongly suggests that upper-level production and advection of E_{p+} from the main convective core is the cause of the elongated layer of E_{p+} ahead of the E_{p+} core. The intracloud energy E_{pic} has more structure in the cloud-column-like structures than does E_{p-}. The former has two columns of maximum values, like the cross section of E_{p-}. However, vertically elongated lobes surround the cloudlike columns in the E_{pic} cross section. These elongated lobes might be the result of vertical advection of E_{pic} energy from different heights and detrainment of cloud mass from the convective updraft into the surrounding air. Moreover, the E_{pic} cross section shows a small area of charging to the west of the main column, whose top portion begins just above the freezing level. This is likely related to falling graupel particles in the volume of descending air behind the trailing stratiform clouds. These falling ice particles intermingle with the relatively shallow convective cell located at about −89.7°, which then leads to charging in the cloud layer just above this lower-level convective core.

Figure 8 shows the probability of detection (POD) and false alarm ratio (FAR) calculated from forecast

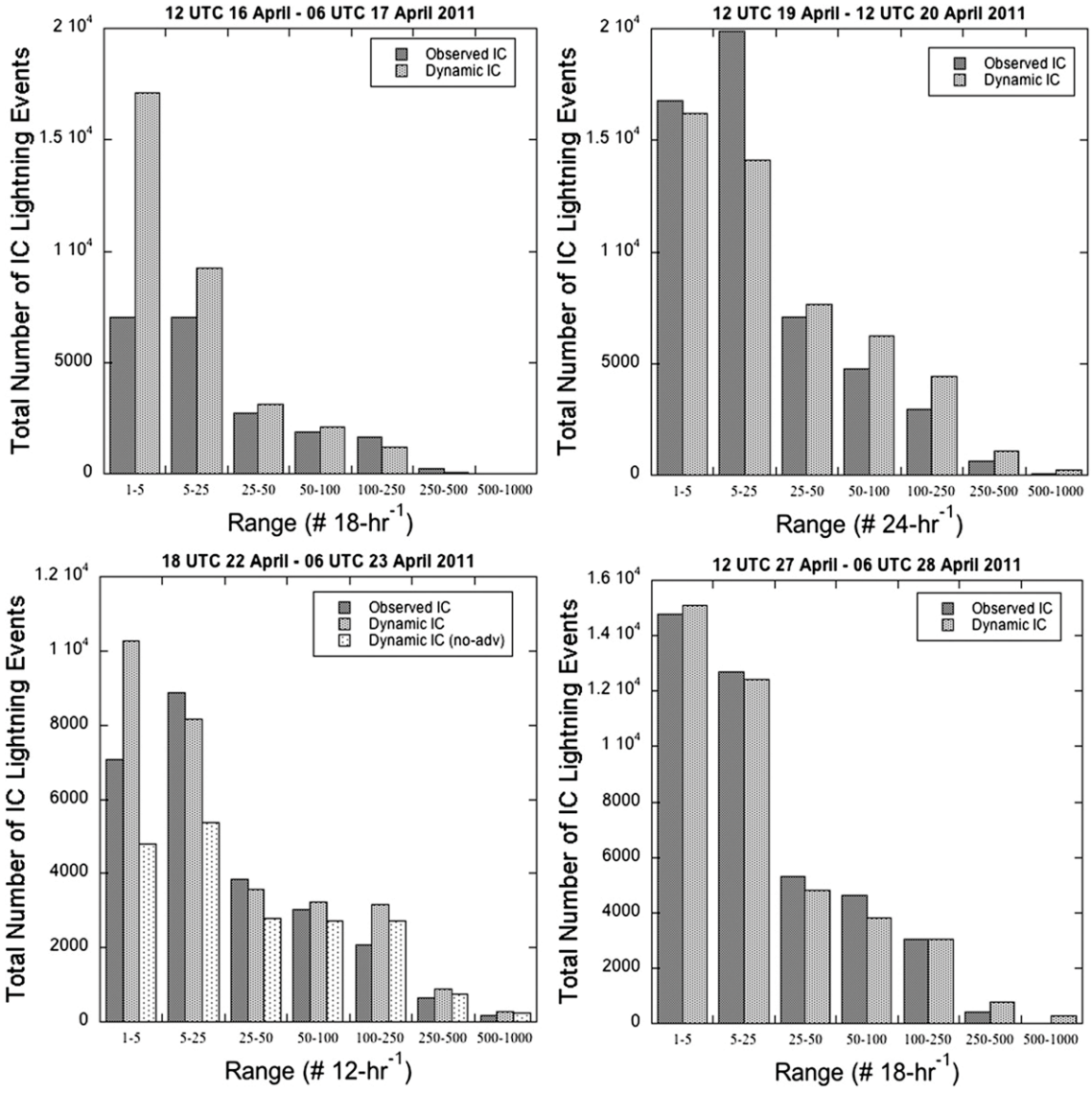

FIG. 4. As in Fig. 2, but for observed vs forecast IC.

cloud-to-ground lightning and observed USPLN cloud-to-ground lightning for the entire simulation event. Results are shown for calculations based on the 4-km simulation grid, a 12 km × 36 km grid overlay. The graphs show results for grid elements with ≥1 cloud-to-ground lightning event and ≥10 lightning events. For the analysis on the 4-km grid, the POD was about 0.5 and was about twice as large as the FAR for grid elements with at least one lightning observation. However, the POD was much less than the FAR for forecasts of grid elements with at least 10 lightning events. For the 12- and 36-km grids, the POD was much larger than the FAR on each grid for both lightning threshold values. The POD was as high as 0.84 for grid elements with at least 10 events in the 36-km overlaid grid. The highest threat scores were found on the 36-km grid, where the threat score was 0.66 (0.60 for ≥10 events) and the bias was 1.07 (1.22). In contrast, the threat score on the 12-km grid was 0.57 (0.42).

c. Comparison with statistical scheme

The statistical scheme described in McCaul et al. (2009) is widely used, and forecasts of total lightning flashes were made for the same case studies described above. The statistical scheme was compared against total lightning flash data, after first grouping the Earth Network stroke data into flashes. We assumed that any stroke or lightning observations observed to be within

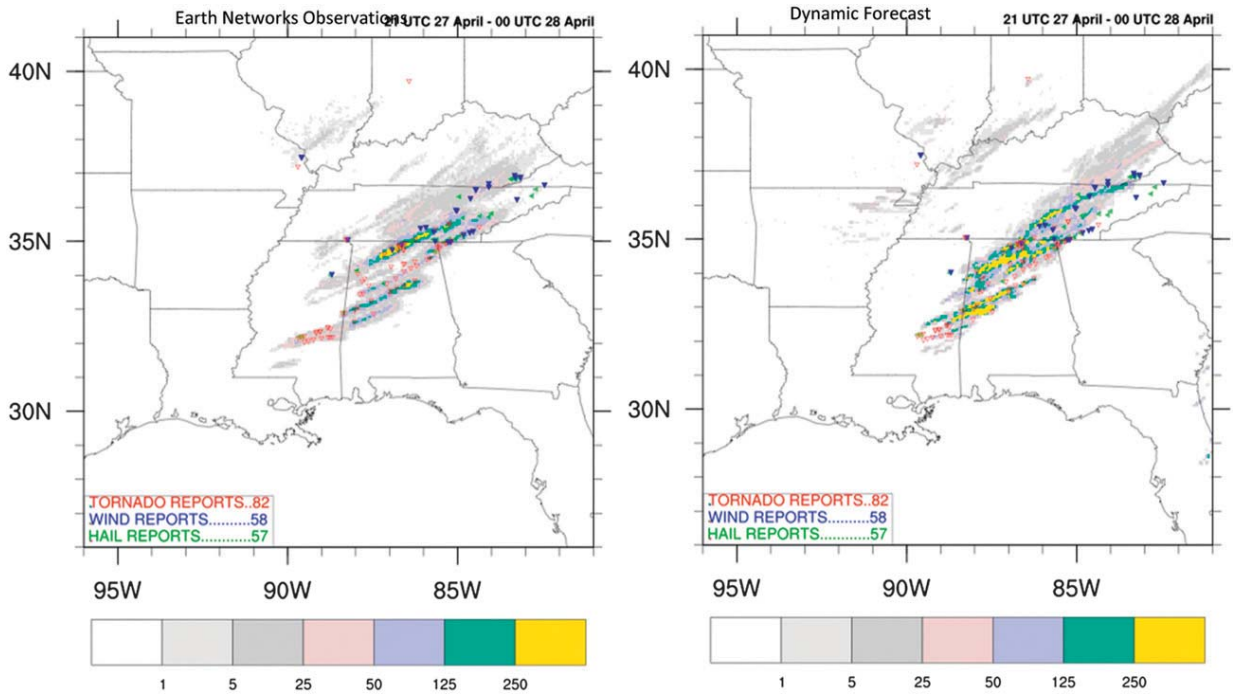

FIG. 5. (left) Observed total lightning overlaid with SPC reports from 2100 UTC 27 Apr until 0000 UTC 28 Apr 2011. (right) Dynamic forecast overlaid with SPC reports for the same time period as in the left panel.

10 km and 2 s of each other were designated as being part of a single flash. Figure 8 shows that the statistical scheme also forecasts the timing of the peak lightning for the Tuscaloosa event, as in the dynamic scheme. However, the total amount of lightning is underforecast by about 50%. Figure 9 shows that there were many more flashes predicted in the range $1 \leq \# < 3$ than were observed. In contrast, the statistical scheme underpredicted the number of flashes in the higher set of range values. These results were typical of other case study days.

Figure 10 compares the POD, FAR, and threat score (TS) for both the dynamic and statistical schemes, calculated for the 36-km grid overlay. The forecasts were compared to cloud-to-ground lightning. The forecast values of lightning in the statistical scheme were compared directly against the WSI data; that is, it was

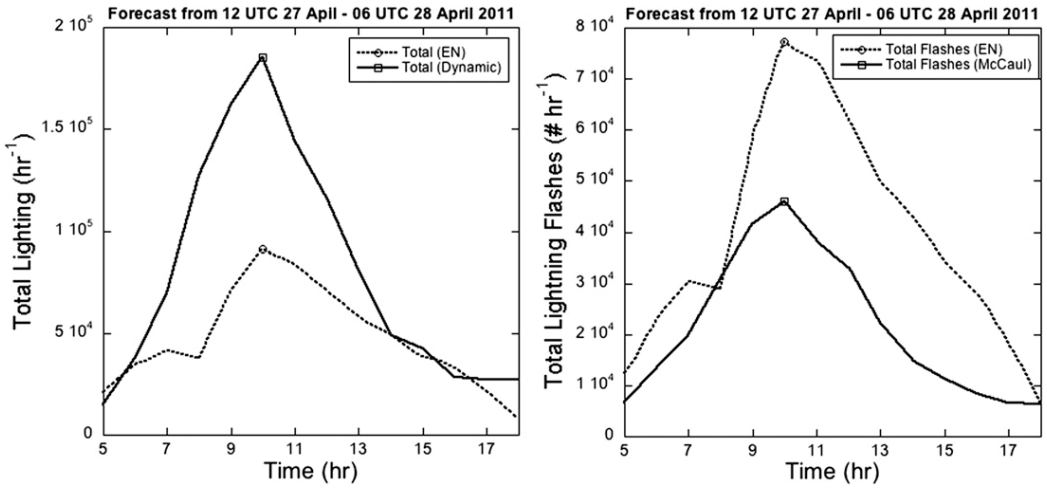

FIG. 6. (left) Observed and dynamically forecast average number of total lighting events in an area within a circular radius 300 km of Tuscaloosa. (right) Observed lightning flash forecasts from the statistical forecast scheme. The observations are from the Earth Network dataset.

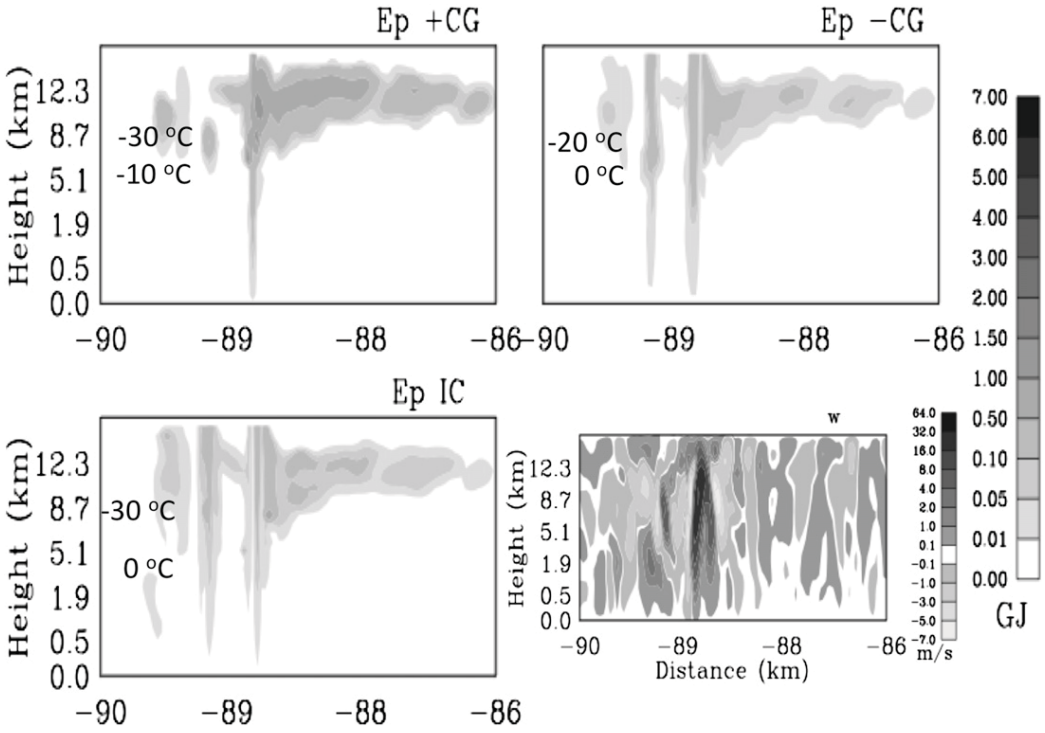

FIG. 7. A snapshot at 2100 UTC 27 April of vertical cross sections of energy and vertical velocity located at 32.32°N (centered near western AL) at the same time instance of Fig. 5. The temperatures mark the approximate height of the corresponding isotherms delineating the bounds of the charging zones for each energy type.

assumed that the percentage of flashes per number of lightning events (~0.5) was the same as the percentage of cloud-to-ground flashes compared to the total number of forecast flashes (note: assuming that the number of cloud-to-ground flashes was ¼—rather than ½ the number of flashes—only had a very minor impact on the scores). The statistical scheme had higher values of POD and FAR than the dynamic scheme for both threshold values of 1 lightning event and 10 lightning events. Due to the relatively large number of false alarms in the statistical scheme, the TS for the statistical scheme was lower than was obtained for the dynamic scheme.

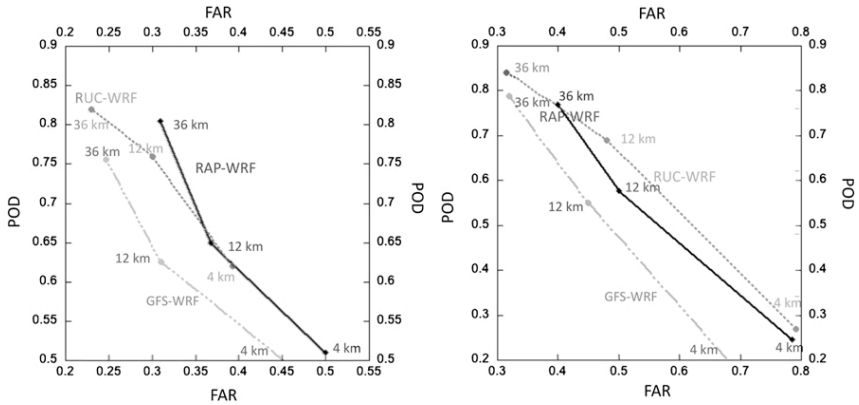

FIG. 8. POD is plotted (vertical axis) against FAR (horizontal axis). Each curve represents a (three point) relative operating characteristic (ROC) curve from the RAP-WRF, RUC-WRF, and GFS-WRF forecasts for the 27 April Tuscaloosa case study event. Each of the points on each curve is labeled to identify POD vs FAR values from the 4-, 12-, and 36-km grid elements. (left) Skill cores for at least one lightning event. (right) Skill scores for at least 10 lightning events.

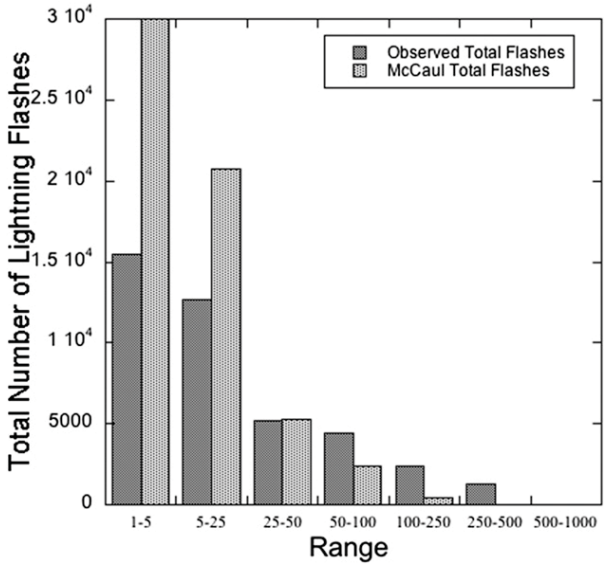

FIG. 9. Observed number of lightning flashes vs statistically forecast number of lightning flashes (McCaul) for the case study day beginning 1200 UTC 27 Apr 2011. The data have been binned over the intervals shown in the graph and the full extent of the values for the smallest bin is not shown.

5. Sensitivity tests

Two additional simulations were produced using RAP (rather than RUC) and GFS forecast data for the Tuscaloosa tornado case. The probability of detection and false alarm ratio are also shown in Fig. 8. Using the RUC data for initial and lateral boundary conditions for the WRF produced higher values of PAR and nearly the same or lower values of FAR on all grids for both lightning forecast thresholds than the other forecast runs. The threat score was 0.66 for at least one event (0.60, at least 10 events) for the RUC. The RAP-forced runs had higher PAR values than the GFS-forced runs; however, the FAR values were also higher. The threat score for the RAP on the 36-km grid was 0.59 (0.50), but 0.60 (0.54) for the GFS for a lightning threshold of at least 1 (10) event per experiment. Another fact to consider, though is that the spinup time in the RAP was lower (3–6 h) compared to 6–9 h in the RUC (not shown), and the GFS.

Table 2 shows observed total lightning, intracloud lightning, and cloud-to-ground lightning versus the forecast values from the control simulation with WSM6 microphysics (and RUC initial conditions), and two simulations with the ''Lin'' microphysics. The study day is also the Tuscaloosa tornado case, and the large ice hydrometeor was set to either graupel or hail in each respective simulation with the Lin microphysics. For both of these simulations, the POD and FAR were worse than those obtained with the WSM6 microphysics for both threshold values (not shown). Moreover, the threat score for a threshold value of 1 on the 12-km grid dropped to 0.50 for the graupel setting and 0.49 for the hail setting, compared to 0.57 for the simulation with WSM6. For a threshold of at least 10 lightning events on the 12-km grid, the threat score was 0.36 for the graupel simulation and 0.32 for the hail simulation. Hence, even though hail was observed in this storm, using a hail simulation did not improve the threat score (or the POD or FAR for that matter). It is suggested that the numbers

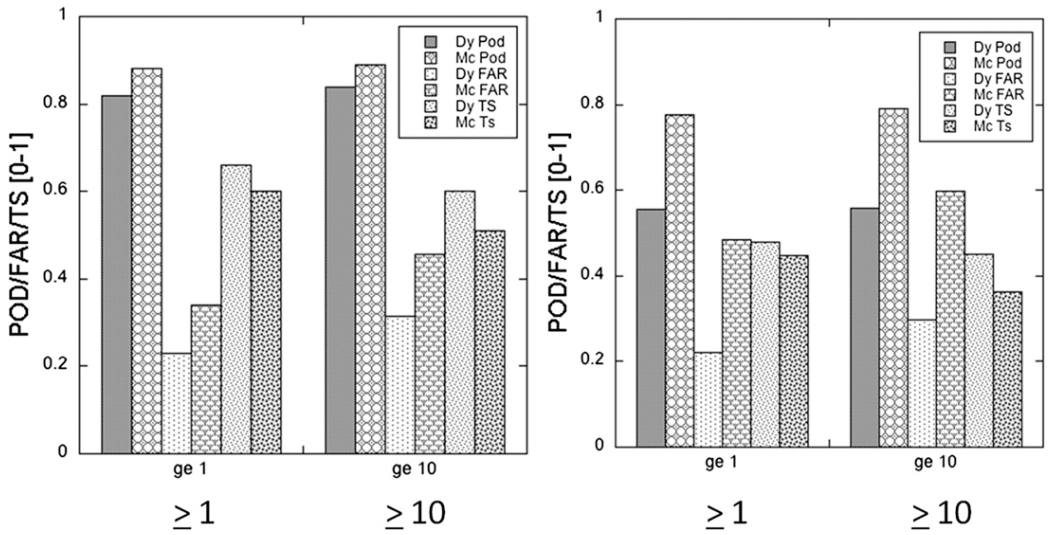

FIG. 10. POD, FAR, and TS values for (left) the Tuscaloosa tornado case (27/28 Apr 2011) and (right) a weakly forced convective case (with relatively few severe weather reports) on 4 Feb 2012. Results are presented for the dynamic scheme and the McCaul scheme for 36-km grid elements with ≥1 or ≥10 CG lightning events.

TABLE 2. Comparison of a forecast of the Tuscaloosa tornado event using WSM6 and Lin microphysics (with either graupel or hail settings). Observations are shown first. The acronym EN stands for Earth Networks total lightning. The USPLN acronym indicates CG measurements. The IC, +CG, and −CG columns show the numbers of 4-km grid elements with lightning observations–forecasts in each range.

Obs					
Range (EN)	Total	IC	Range (USPLN)	+CG	−CG
1–5	14 601	14 876	1–3	1354	14 570
5–25	12 936	12 683	3–5	0	3082
25–50	5400	5288	5–10	0	3792
50–100	4857	4618	10–25	0	3126
100–250	3526	3032	25–50	0	790
250–500	549	431	50–100	0	109
500–1000	39	20	100–250	0	2
WSM6					
Range (EN)	Total	IC	Range (USPLN)	+CG	−CG
1–5	14 721	14 721	1–3	2905	14 820
5–25	13 666	14 057	3–5	140	4100
25–50	6280	6300	5–10	42	5536
50–100	5695	5375	10–25	0	4076
100–250	4389	4003	25–50	0	893
250–500	1144	934	50–100	0	128
500–1000	207	146	100–250	0	5
Lin with graupel setting					
Range (EN)	Total	IC	Range (USPLN)	+CG	−CG
1–5	13 398	14 707	1–3	775	16 888
5–25	14 163	14 012	3–5	74	4411
25–50	5735	5379	5–10	26	4447
50–100	4103	3722	10–25	0	2509
100–250	2515	2214	25–50	0	462
250–500	515	417	50–100	0	89
500–1000	149	131	100–250	0	0
Lin with hail setting					
Range (EN)	Total	IC	Range (USPLN)	+CG	−CG
1–5	13 258	14 095	1–3	575	15 063
5–25	13 286	13 264	3–5	12	2836
25–50	4446	4150	5–10	1	2527
50–100	2965	2445	10–25	0	1524
100–250	1665	1506	25–50	0	403
250–500	440	353	50–100	0	62
500–1000	70	45	100–250	0	0

of total forecast events in the different ranges with the hail setting were less than with the graupel setting because the residence time of the hail was smaller than the residence time of graupel, and this reduced the overall charging of the cloud layers.

The previous set of simulations examined the accuracy of the forecast algorithm during severe weather events. In another simulation, the forecast accuracy was evaluated during an early February nonsevere event (Table 3). Lightning occurred over Texas, Alabama, Louisiana, Arkansas, and Mississippi. There were just four severe wind reports, five hail reports, and two tornado reports from 0300 UTC 4 February until 0000 UTC 5 February 2012. Figure 9 also shows the POD, FAR, and TS from the dynamic and statistical schemes. The statistical scheme produced higher values of POD and FAR than did the dynamic scheme, but the TS for the dynamic scheme were larger than those for the statistical scheme for both lightning threshold values.

Another set of experiments used a grid with 3-km rather than 4-km grid spacing. Table 4 suggests that when the algorithm used the coefficients shown in Table 1, that the forecast has a positive bias. Table 4 also shows the results obtained when the algorithm runs using the set of coefficients at 80% of their values in Table 1. These results are closer to the observed values in all ranges. One should keep in mind that the energy generated by the algorithm is proportional to Qw^2, but inversely proportional to the grid volume, which in the 3-km grid is only 56% of the volume of a 4-km grid. The better fit obtained with the reduced values of the coefficients suggests that higher values of Qw^2 produce a greater impact on the energy of the grid than the decrease in grid-scale energy associated with the reduced volume of the 3-km grid.

A series of operational forecasts was made during the winter of 2012 (Table 5). Skill scores for each are tabulated for forecast versus observed lightning over the time period of the forecast. The TS score for at least one lightning event was at least 0.5 for six of the seven forecasts. The TS for at least 10 lightning events was at least 0.5 for two of the seven forecasts. The two days (29 February and 27 April) on which the skill scores were higher for at least 10 lighting events corresponded to days with a number of severe weather reports, indicating more organized convection. On 2 March, however, there were also a number of severe weather reports—yet the TS score for at least lightning events was low. Further examination of this forecast indicated that the overall pattern of lightning matched quite well the observed pattern, but the intensity of the forecast convection (as indicated by the lightning) was less than observed. Hence, the skill scores depend not only on the accuracy of the lightning scheme, but also on the forecast of convection and lightning-producing clouds in the operational runs.

6. Discussion and conclusions

A dynamically based algorithm was implemented into the WRF to predict the occurrence of and produce

TABLE 3. As in Table 2, but for observed and forecast lightning values on 4 Feb 2012 made using the "standard" WSM6 microphysics.

Observed					
Range (EN)	Total	IC	Range (USPLN)	+CG	−CG
1–5	11 939	12 341	1–3	1801	11 709
5–25	9300	8786	3–5	3	2348
25–50	2766	2346	5–10	0.	2469
50–100	1642	1271	10–25	0.	1870
100–250	743	579	25–50	0.	433
250–500	195	158	50–100	0.	162
500–1000	67	60	100–250	0	20
Dynamic					
Range (EN)	Total	IC	Range (USPLN)	+CG	−CG
1–5	10 241	11 120	1–3	25	9399
5–25	7751	7306	3–5	7	1436
25–50	1802	1587	5–10	2	1090
50–100	957	827	10–25	4	487
100–250	475	401	25–50	0	65
250–500	76	65	50–100	0	21
500–1000	25	22	100–250	0	5

TABLE 4. Forecasts made using 3-km grid resolution. In the first simulation, the charging coefficients were the same as in Table 1. In the second, the charging coefficients were reduced by 20%.

Observations					
Range (EN)	Total	IC	Range (USPLN)	+CG	−CG
1–5	28 128	28 499	1–3	1230	22 540
5–25	22 119	21 687	3–5	1	4399
25–50	8750	8503	5–10	0	4773
50–100	6119	5534	10–25	0	2747
100–250	2412	1942	25–50	0	329
250–500	127	84	50–100	0	11
500–1000	0	0	100–250	0	0
Dynamic (1)					
Range (EN)	Total	IC	Range (USPLN)	+CG	−CG
1–5	27 238	28 068	1–3	2469	28 345
5–25	26 250	27 075	3–5	28	7374
25–50	11 556	11 347	5–10	4	7645
50–100	8788	8126	10–25	0	3996
100–250	5112	4483	25–50	0	491
250–500	768	604	50–100	0	15
500–1000	55	28	100–250	0	0
Dynamic (2)					
Range (EN)	Total	IC	Range (USPLN)	+CG	−CG
1–5	28 406	29 233	1–3	1290	27 714
5–25	26 298	27 030	3–5	6	6478
25–50	10 893	10 492	5–10	0	5785
50–100	7175	6626	10–25	0	2585
100–250	3639	3106	25–50	0	194
250–500	409	302	50–100	0	3
500–1000	11	9	100–250	0	0

forecast maps for cloud-to-ground (positive and negative) and intracloud lightning. The scheme uses the dynamic and microphysics fields from the WRF cloud-resolving model to calculate the electrical potential energy for +GC, −CG, and IC lighting, from which the number of CG lightning strokes and IC events are, respectively, forecast. The algorithm was first tested on four case study events, which were mostly evaluated based on the forecast number of lightning events versus the observed number of events in certain ranges (bins). Skill scores were calculated for the case study of 27 April 2011 and additional operational forecasts were done during the winter of 2012 using RAP boundary conditions. The analysis of these case study events indicates that the lightning forecast algorithm shows promise for being able to predict the occurrence of cloud-to-ground positive and negative lightning and intracloud lighting.

A sensitivity test was conducted to examine the potential impact of using a microphysics scheme with hail versus graupel. The use of the hail option led to a reduction in forecast lightning intensity. Emersic et al. (2011) discuss lightning activity in a hail-producing storm. They note that the production of wet hail can lead to a lightning "hole," as wet hail is not conducive to charging. Here, though, we believe that the reduced residence time of hail compared to graupel was the most likely reason lightning values were reduced relative to the test with the graupel setting. A test comparing the lightning forecast with 3-km versus 4-km grid spacing used in the experiments described above indicated that the algorithm can also be used at both resolutions; however, the charging coefficients were changed to make the results more similar to each other. The lighting algorithm was not tried at 1.3-km grid resolution. Dahl et al. (2011) highlight the importance of scale in thunderstorm clouds as a determining factor in lightning production. Hence, it would probably be more appropriate to make the lightning calculations on the 4-km grid that is likely to host any 1.3-km higher-resolution grid.

Combined with other indicators for severe weather—like helicity—the lightning forecast could possibly be used to more accurately predict the timing and location of severe weather several hours or longer in advance. This could narrow the time and spatial window for severe weather watches.

The algorithm simulated the total number of positive cloud-to-ground strokes quite well, including forecasting the number of grid elements within certain ranges of +CG per event. Yet, we should mention that Curran and Rust (1992) and other observational studies have

TABLE 5. Date of forecast and total number of CG events (from USPLN) and the skill scores for different forecasts. The skill scores are for 36-km areas superimposed on the forecast 4-km grid. The boundary conditions used were obtained from the RAP. In the first simulation, there was no spinup prior to the 18-h simulation. In the others, there was a 3-h spinup where hourly RAP reanalysis data were used to nudge the model with FDDA. The (operational) forecast that followed did not use FDDA, and the RAP boundary conditions used as lateral boundary conditions were at 3-h intervals. Skill scores for two threshold values are shown: at least 1 CG event per forecast per grid and at least 10 CG events per forecast per grid.

Date	Total No. of CG events	
27 Apr 2011	157 348	
Score type	$\geqq 1$	$\geqq 10$
POD	0.81	0.77
FAR	0.31	0.40
TS	0.59	0.51
Bias	1.17	1.28
21 Jan 2012	47 563	
POD	0.65	0.48
FAR	0.234	0.25
TS	0.54	0.41
Bias	0.84	0.65
29 Feb 2012	81 133	
POD	0.798	0.70
FAR	0.24	0.39
TS	0.63	0.52
Bias	1.053	1.04
2 Mar 2012	87 153	
POD	0.60	0.52
FAR	0.263	0.35
TS	0.50	0.40
Bias	0.817	0.80
8 Mar 2012	50 797	
POD	0.69	0.59
FAR	0.355	0.39
TS	0.50	0.43
Bias	1.06	0.96
9 Mar 2012	68 537	
POD	0.60	0.59
FAR	0.49	0.50
TS	0.38	0.37
Bias	1.16	1.19
11 Mar 2012	33 845	
POD	0.71	0.61
FAR	0.30	0.38
TS	0.54	0.44
Bias	1.02	0.984

shown that supercell storms can be associated with relatively low precipitation rates (at least to start) and mostly positive cloud-to-ground lightning strikes, which are then followed by mostly negative cloud-to-ground lightning strikes during the mature stage of the supercell. Stolzenburg (1994) confirmed that exceptionally tall Great Plains storms initially produce mostly +CG lightning. Further, MacGorman and Burgess (1994) noted that observed positive CG lightning flashes were mostly associated with large hail, and Lang et al. (2004) also identified large hail as being associated with positive cloud-to-ground lightning in convective clouds, multicell storms, and supercell storms. We are hoping to investigate how the forecast algorithm predicts positive cloud-to-ground lightning using additional microphysical schemes with hail.

Rakov (2003) notes that many winter storms are associated with predominately positive cloud-to-ground lightning and may actually have a unipolar charge structure. This scheme, as currently formulated, cannot forecast the ratio of positive to negative lightning associated with the unipolar charge structure of wintertime lightning events, or perhaps storms for which the positive CG events occur from near cloud base, rather than in anvils or stratiform cloud.

As noted, the implementation of an algorithm to calculate lightning strokes in WRF requires greater computational expense than using statistical formulations to calculate the lightning from the WRF model output. The analysis of lightning forecasts comparing the dynamic approach to the statistical scheme suggested that the former better reproduces the distribution of lightning, as well as being more sensitive to changes in the intensity of convection. There was a large positive bias, for example, in the statistical scheme's lightning flash prediction for grid elements with values $1 \leq \# < 10$, while there was an underprediction of lightning when there were more than 50 flashes at each grid. Hence, in the analysis of the Tuscaloosa tornado event (27 April 2011), the statistical scheme underestimated the peak flash rate by at least a factor of 2.

In contrast, the dynamic scheme better produced the peak total lightning. One reason that the statistical scheme might produce too many low flash rates is because the scheme produces flashes anytime certain thresholds are reached, regardless of whether a previous flash had recently occurred at that grid element. On the other hand, the statistical scheme uses the graupel flux in an atmospheric layer defined at a single temperature rather than calculating the flash rate based on the graupel flux within a certain temperature range—like the dynamic scheme. Hence, the statistical scheme cannot represent as well the potential charging in multiple layers that affects flash rate, especially in deep convection. An additional simulation using the dynamic scheme with advection turned off (and all potential electric energy converted to flashes or dissipated in a single time step) also showed the importance of advection of energy from one grid element to another as a producer of lighting. Additional comparisons to those simulations made with the Earth Network data could include cloud lightning observed with the Lightning

Detection Network (LINET) system in Europe (i.e., Betz et al. 2009).

The implementation of a lightning algorithm in WRF has the potential to improve lightning prediction and contribute to public safety, as well as improving private and government preparation time for impending severe weather. The parameters used to calculate the growth of electrical potential energy, the threshold energy values for which cloud-to-ground strokes or cloud lightning occur, and the time scales of the strokes and cloud lightning are all physically based parameters whose values can be fine-tuned based on additional case study simulations.

Acknowledgments. We thank WSI and Earth Networks for providing the lightning data for this study, and NCDC for providing the system infrastructure to make it convenient to download and use RUC data.

REFERENCES

American Meteorological Society, 1924a: Lightning explodes dynamite. *Mon. Wea. Rev.,* **52,** 313.

——, 1924b: Loss of forty-seven head of cattle by a single lightning bolt. *Mon. Wea. Rev.,* **52,** 452.

Ashley, W. S., and C. W. Gilson, 2009: A reassessment of U.S. lightning mortality. *Bull. Amer. Meteor. Soc.,* **90,** 1501–1518.

Barthe, C., and J.-P. Pinty, 2007: Simulation of a supercellular storm using a three-dimensional mesoscale model with an explicit lightning flash scheme. *J. Geophys. Res.,* **112,** D06210, doi:10.1029/2006JD007484.

Betz, H. D., K. Schmidt, and W. P. Oettinger, 2009: LINET—An international VLF/LF lightning detection network in Europe. *Lightning: Principles, Instruments and Applications: Review of Modern Lightning Research,* H. D. Betz et al., Eds., Springer, 115–140.

Branick, M. L., and C. A. Doswell III, 1992: An observation of the relationship between supercell structure and lightning ground-strike polarity. *Wea. Forecasting,* **7,** 143–149.

Bright, D. R., M. S. Wandishin, R. E. Jewell, and S. J. Weiss, 2005: A physically based parameter for lightning prediction and its calibration in ensemble forecasts. Preprints, *Conf. on Meteor. Applications of Lightning Data,* San Diego, CA, Amer. Meteor. Soc., 4.3. [Available online at http://ams.confex.com/ams/pdfpapers/84173.pdf.]

Burrows, W. R., C. Price, and L. J. Wilson, 2005: Warm season lightning probability prediction for Canada and the northern United States. *Wea. Forecasting,* **20,** 971–988.

Chen, F., and J. Dudhia, 2001a: Coupling an advanced land surface–hydrology model with the Penn State–NCAR MM5 modeling system. Part I: Model implementation and sensitivity. *Mon. Wea. Rev.,* **129,** 569–585.

——, and ——, 2001b: Coupling an advanced land surface–hydrology model with the Penn State–NCAR MM5 modeling system. Part II: Preliminary model validation. *Mon. Wea. Rev.,* **129,** 587–604.

Curran, E. B., and W. D. Rust, 1992: Positive ground flashes produced by low-precipitation thunderstorms in Oklahoma on 26 April 1984. *Mon. Wea. Rev.,* **120,** 544–553.

——, R. L. Holle, and R. E. López, 2000: Lightning casualties and damages in the United States from 1959 to 1994. *J. Climate,* **13,** 3448–3464.

Dahl, J. M. L., H. Höller, and U. Schumann, 2011: Modeling the flash rate of thunderstorms. Part I: Framework. *Mon. Wea. Rev.,* **139,** 3093–3111.

Dudhia, J., 1989: Numerical study of convection observed during the Winter Monsoon Experiment using a mesoscale two-dimensional model. *J. Atmos. Sci.,* **46,** 3077–3107.

——, S.-Y. Hong, and K.-S. Lim, 2008: A new method for representing mixed-phase particle fall speeds in bulk microphysics parameterizations. *J. Meteor. Soc. Japan,* **86,** 33–44.

Emersic, C., P. L. Heinselman, D. R. MacGorman, and E. C. Bruning, 2011: Lightning activity in a hail-producing storm observed with phased-array radar. *Mon. Wea. Rev.,* **139,** 1809–1825.

Fierro, A. O., M. S. Gilmore, E. R. Mansell, L. J. Wicker, and J. M. Straka, 2006: Electrification and lightning in an idealized boundary-crossing supercell simulation of 2 June 1995. *Mon. Wea. Rev.,* **134,** 3149–3172.

——, L. M. Leslie, E. R. Mansell, J. M. Straka, D. R. MacGorman, and C. Ziegler, 2007: A high-resolution simulation of the microphysics and electrification in an idealized hurricane-like vortex. *Meteor. Atmos. Phys.,* **98,** 13–33.

——, ——, ——, and ——, 2008: Numerical simulations of the microphysics and electrification of the weakly electrified 9 February 1993 TOGA COARE squall line: Comparisons with observations. *Mon. Wea. Rev.,* **136,** 364–379.

Givati, A., B. Lynn, Y. Liu, and A. Rimmer, 2012: Using the WRF model in an operational streamflow forecast system for the Jordan River. *J. Appl. Meteor. Climatol.,* **51,** 285–299.

Gremillion, M. S., and R. E. Orville, 1999: Thunderstorm characteristics of cloud-to-ground lightning at the Kennedy Space Center, Florida: A study of lightning initiation signatures as indicated by the WSR-88D. *Wea. Forecasting,* **14,** 640–649.

Helsdon, J. H., Jr., and R. D. Farley, 1987: A numerical study of a Montana thunderstorm: 2. Model results versus observations involving electrical aspects. *J. Geophys. Res.,* **92** (D5), 5661–5675.

Hodanish, S., R. L. Holle, and D. T. Lindsey, 2004: A small updraft producing a fatal lightning flash. *Wea. Forecasting,* **19,** 627–632.

Holle, R. L., R. E. López, L. J. Arnold, and J. Endres, 1996: Insured lightning-caused property damage in three western states. *J. Appl. Meteor.,* **35,** 1344–1351.

——, ——, and B. C. Navarro, 2005: Deaths, injuries, and damages from lightning in the United States in the 1890s in comparison with the 1990s. *J. Appl. Meteor.,* **44,** 1563–1573.

Hondl, K. D., and M. D. Eilts, 1994: Doppler radar signatures of developing thunderstorms and their potential to indicate the onset of cloud-to-ground lightning. *Mon. Wea. Rev.,* **122,** 1818–1836.

Janjić, Z. I., 2002: Nonsingular implementation of the Mellor–Yamada level 2.5 scheme in the NCEP Meso Model. NCEP Office Note 437, 61 pp.

Kain, J. S., 2004: The Kain–Fritsch convective parameterization: An update. *J. Appl. Meteor.,* **43,** 170–181.

——, and J. M. Fritsch, 1993: Convective parameterization for mesoscale models: The Kain–Fritsch scheme. *The Representation of Cumulus Convection in Numerical Models, Meteor. Monogr.,* No. 46, Amer. Meteor. Soc., 165–170.

Kitagawa, N., and K. Michimoto, 1994: Meteorological and electrical aspects of winter thunderclouds. *J. Geophys. Res.,* **99** (D5), 10 713–10 721.

Kohn, M., E. Galanti, C. Price, K. Lagouvardos, and V. Kotroni, 2010: Now-casting thunderstorms in the Mediterranean region using lightning data. *Atmos. Res.,* **100,** 489–502.

Krehbiel, P. R., J. A. Riousset, V. P. Pasko, R. J. Thomas, W. Rison, M. A. Stanley, and H. E. Edens, 2008: Upward electrical discharges from thunderstorms. *Nat. Geosci.,* **1,** 233–237.

Kuhlman, K. M., C. L. Ziegler, E. R. Mansell, D. R. MacGorman, and J. M. Straka, 2006: Numerically simulated electrification and lightning of the 29 June 2000 STEPS supercell storm. *Mon. Wea. Rev.,* **134,** 2734–2757.

Lang, T. J., and Coauthors, 2004: The Severe Thunderstorm Electrification and Precipitation Study. *Bull. Amer. Meteor. Soc.,* **85,** 1107–1125.

López, R. E., and R. L. Holle, 1996: Fluctuations of lightning casualties in the United States: 1959–1990. *J. Climate,* **9,** 608–615.

——, ——, and T. A. Heitkamp, 1995: Lightning casualties and property damage in Colorado from 1950 to 1991 based on *Storm Data*. *Wea. Forecasting,* **10,** 114–126.

Lynn, B. H., and Y. Yair, 2010: Prediction of lightning flash density with the WRF model. *Adv. Geosci.,* **23,** 11–16.

MacGorman, D. R., and K. E. Nielsen, 1991: Cloud-to-ground lightning in a tornadic storm on 8 May 1986. *Mon. Wea. Rev.,* **119,** 1557–1574.

——, and D. W. Burgess, 1994: Positive cloud-to-ground lightning in tornadic storms and hailstorms. *Mon. Wea. Rev.,* **122,** 1671–1697.

——, and W. D. Rust, 1998: *The Electrical Nature of Storms*. Oxford University Press, 422 pp.

——, J. M. Straka, and C. L. Ziegler, 2001: A lightning parameterization for numerical cloud models. *J. Appl. Meteor.,* **40,** 459–478.

Mansell, E. R., D. R. MacGorman, C. L. Ziegler, and J. M. Straka, 2002: Simulated three-dimensional branched lighting in a numerical thunderstorm model. *J. Geophys. Res.,* **107,** 4075, doi:10.1029/2000JD000244.

——, C. L. Ziegler, and E. C. Bruning, 2010: Simulated electrification of a small thunderstorm with two-moment bulk microphysics. *J. Atmos. Sci.,* **67,** 171–194.

Mazany, R. A., S. Businger, S. I. Gutman, and W. Roeder, 2002: A lightning prediction index that utilizes GPS integrated precipitable water vapor. *Wea. Forecasting,* **17,** 1034–1047.

McCaul, E. W., S. J. Goodman, K. M. LaCasse, and D. J. Cecil, 2009: Forecasting lightning threat using cloud-resolving model simulations. *Wea. Forecasting,* **24,** 709–729.

Mellor, G. L., and T. Yamada, 1982: Development of a turbulence closure model for geophysical fluid problems. *Rev. Geophys.,* **20,** 851–875.

Mlawer, E. J., S. J. Taubman, P. D. Brown, M. J. Iacono, and S. A. Clough, 1997: Radiative transfer for inhomogeneous atmosphere: RRTM, a validated correlated-k model for the long-wave. *J. Geophys. Res.,* **102** (D14), 16 663–16 682.

Mosier, R. M., C. Schumacher, R. E. Orville, and L. D. Carey, 2011: Radar nowcasting of cloud-to-ground lightning over Houston, Texas. *Wea. Forecasting,* **26,** 199–212.

Nielsen, K. E., R. A. Maddox, and S. V. Vasiloff, 1994: The evolution of cloud-to-ground lightning within a portion of the 10–11 June 1985 squall line. *Mon. Wea. Rev.,* **122,** 1809–1817.

Parker, M. D., S. A. Rutledge, and R. H. Johnson, 2001: Cloud-to-ground lightning in linear mesoscale convective systems. *Mon. Wea. Rev.,* **129,** 1232–1242.

Pinty, J.-P., and C. Barthe, 2008: Ensemble simulation of the lightning flash variability in a 3D cloud model with parameterizations of cloud electrification and lightning flashes. *Mon. Wea. Rev.,* **136,** 380–387.

Price, C., 2008: Lightning sensors for observing, tracking and nowcasting severe weather. *Sensors,* **8,** 157–170.

——, and D. Rind, 1994: Modeling global lightning distributions in a general circulation model. *Mon. Wea. Rev.,* **122,** 1930–1939.

Qie, X., T. Zhang, C. Chen, G. Zhang, T. Zhang, and W. Wei, 2005: The lower positive charge center and its effect on lightning discharges on the Tibetan Plateau. *Geophys. Res. Lett.,* **32,** L05814, doi:10.1029/2004GL022162.

Rakov, V. A., 2003: A review of positive and bipolar lightning discarges. *Bull. Amer. Meteor. Soc.,* **84,** 767–776.

——, and M. A. Uman, 2003: *Lightning: Physics and Effects*. Cambridge University Press, 700 pp.

Rorig, M. L., and S. A. Ferguson, 2002: The 2000 fire season: Lightning-caused fires. *J. Appl. Meteor.,* **41,** 786–791.

Rutledge, S. A., C. Lu, and D. R. MacGorman, 1990: Positive cloud-to-ground lightning in mesoscale convective systems. *J. Atmos. Sci.,* **47,** 2085–2100.

Saunders, C. P. R., 2008: Charge separation mechanisms in clouds. *Space Sci. Rev.,* **137,** 335–354, doi:10.1007/s11214-008-09345-0.

Saxen, T. R., and Coauthors, 2008: The Operational Mesogamma-Scale Analysis and Forecast System of the U.S. Army Test and Evaluation Command. Part IV: The White Sands Missile Range Auto-Nowcast System. *J. Appl. Meteor. Climatol.,* **47,** 1123–1139.

Scavuzzo, C. M., and G. M. Caranti, 1996: Thunderstorm electrification analysis: The dependence on the temperature–LWC diagram. *J. Atmos. Sci.,* **53,** 349–358.

Schultz, C. J., W. A. Petersen, and L. D. Carey, 2009: Preliminary development and evaluation of lightning jump algorithms for the real-time detection of severe weather. *J. Appl. Meteor. Climatol.,* **48,** 2543–2563.

Schuur, T. J., W. D. Rust, B. F. Smull, and T. C. Marshall, 1991: Electrical and kinematic structure of the stratiform precipitation region trailing an Oklahoma squall line. *J. Atmos. Sci.,* **48,** 825–842.

Seroka, G. N., R. E. Orville, and C. Schumacher, 2012: Radar nowcasting of total lightning over the Kennedy Space Center. *Wea. Forecasting,* **27,** 189–204.

Shafer, M. A., D. R. MacGorman, and F. H. Carr, 2000: Cloud-to-ground lightning throughout the lifetime of a severe storm system in Oklahoma. *Mon. Wea. Rev.,* **128,** 1798–1816.

Shafer, P. E., and H. E. Fuelberg, 2008: A perfect prognosis scheme for forecasting warm-season lightning over Florida. *Mon. Wea. Rev.,* **136,** 1817–1846.

Short, D. A., J. E. Sardonia, W. C. Lambert, and M. M. Wheeler, 2004: Nowcasting thunderstorm anvil clouds over Kennedy Space Center and Cape Canaveral Air Force Station. *Wea. Forecasting,* **19,** 706–713.

Stern, A. D., R. H. Brady, P. D. Moore, and G. M. Carter, 1994: Identification of aviation weather hazards based on the integration of radar and lightning data. *Bull. Amer. Meteor. Soc.,* **75,** 2269–2280.

Stolzenburg, M., 1994: Observations of high ground flash densities of positive lightning in summertime thunderstorms. *Mon. Wea. Rev.,* **122,** 1740–1750.

Tessendorf, S. A., K. C. Wiens, and S. A. Rutledge, 2007: Radar and lightning observations of the 3 June 2000 electrically inverted storm from STEPS. *Mon. Wea. Rev.,* **135,** 3665–3681.

van den Broeke, M. S., D. M. Schultz, R. H. Johns, J. S. Evans, and J. E. Hales, 2005: Cloud-to-ground lightning production in strongly forced, low-instability convective lines associated with damaging wind. *Wea. Forecasting,* **20,** 517–530.

Wallmann, J., R. Milne, C. Smallcomb, and M. Mehle, 2010: Using the 21 June 2008 California lightning outbreak to improve dry lightning forecast procedures. *Wea. Forecasting,* **25,** 1447–1462.

Weisman, M. L., W. C. Skamarock, and J. B. Klemp, 1997: The resolution dependence of explicitly modeled convective systems. *Mon. Wea. Rev.,* **125,** 527–548.

Weygandt, S. S., S. G. Benjamin, T. G. Smirnova, and J. M. Brown, 2008: Assimilation of radar reflectivity data using a diabatic digital filter within the Rapid Update Cycle. Preprints, *12th Conf. on IOAS-AOLS,* New Orleans, LA, Amer. Meteor. Soc., 8.4. [Available online at http://ams.confex.com/ams/pdfpapers/134081.pdf.]

Wiens, K. C., S. A. Rutledge, and S. A. Tessendorf, 2005: The 29 June 2000 supercell observed during STEPS. Part II: Lightning and charge structure. *J. Atmos. Sci.,* **62,** 4151–4177.

Williams, E. R., 1989: The tripole structure of thunderstorms. *J. Geophys. Res.,* **94** (D11), 13 151–13 167.

Yair, Y., B. H. Lynn, C. Price, V. Kotroni, K. Lagouvardos, E. Morin, A. Mugnai, and M. C. Llasat, 2010: Predicting the potential for lightning activity in Mediterranean storms based on the Weather Research and Forecasting (WRF) model dynamic and microphysical fields. *J. Geophys. Res.,* **115,** D04205, doi:10.1029/2008JD010868.

Yang, Y. H., and P. King, 2010: Investigating the potential of using radar echo reflectivity to nowcast cloud-to-ground lightning initiation over southern Ontario. *Wea. Forecasting,* **25,** 1235–1248.